

# a journal of mathematics

Rhombic planform nonlinear stability analysis of an ion-sputtering evolution equation

Sydney Schmidt, Stephanie Kolden, Bonni Dichone and David Wollkind





# Rhombic planform nonlinear stability analysis of an ion-sputtering evolution equation

Sydney Schmidt, Stephanie Kolden, Bonni Dichone and David Wollkind

(Communicated by Martin J. Bohner)

A damped Kuramoto–Sivashinsky equation describing the deviation of an interface from its mean planar position during normal-incidence ion-sputtered erosion of a semiconductor or metallic solid surface is derived and the magnitude of the gradient in its source term is approximated so that it will be of a modified Swift–Hohenberg form. Next, one-dimensional longitudinal and two-dimensional rhombic planform nonlinear stability analyses of the zero deviation solution to this equation are performed, the former being a special case of the latter. The predicted theoretical morphological stability results of these analyses are then shown to be in very good qualitative and quantitative agreement with relevant experimental evidence involving the occurrence of smooth surfaces, ripples, checkerboard arrays of pits, and uniform distributions of islands or holes once the concept of lower- and higher-threshold rhombic patterns is introduced based on the mean interfacial position.

## 1. Introduction and formulation of the problem

Consider the following nondimensional spatiotemporal model evolution equation for h(x, y, t), a dimensionless deviation of a thin solid film surface from its mean planar position, where  $t \equiv \text{time}$  and  $(x, y) \equiv \text{a}$  transverse laboratory Cartesian coordinate system:

$$h_t + 4\nabla^2 h + 2\nabla^4 h + \beta[\sinh(2h) - \alpha h^2] = 0, \quad \alpha \in \mathbb{R}, \ \beta > 0.$$

Here  $\alpha$  and  $\beta$  are dimensionless combinations of experimental and material parameters. Then, consistent with our nonlinear stability analyses, retaining only terms through third order in

$$\sinh(2h) \sim (2h) + \frac{1}{6}(2h)^3 = 2h + \frac{4}{3}h^3,$$

MSC2020: 35B35, 35B36, 35R35, 74A50, 74K35.

*Keywords*: ion-sputtered erosion, Kuramoto–Sivashinsky equation, Swift–Hohenberg equation, nonlinear stability analysis, rhombic pattern formation.

that equation is reduced to its truncated form

$$h_t + 4\nabla^2 h + 2\nabla^4 h + \beta (2h - \alpha h^2 + \frac{4}{3}h^3) = 0.$$

Let us provide a phenomenological derivation of this model equation. Sputtering, the removal of material from the surface of semiconductor or metallic solids through ion bombardment, is an important thin-film processing technique (reviewed in [Makeev et al. 2002]). The erosion rate for such surfaces can be characterized by the ion flux, defined as the number of particles arriving per unit area per unit time, and the sputtering yield, defined as the amount of material leaving the surface per unit incident particle. In the sputtering process the incoming ions penetrate the solid and transfer their kinetic energy to the substrate material by inducing a collision cascade that allows some of the latter to gain sufficient energy to be removed from the surface or sputtered. One might suspect that erosion of this sort would tend to erase every possible interfacial feature and give rise to only a uniformly smooth morphology; however, under certain circumstances, periodic patterns are actually etched on the surface. That spontaneous self-organization is generated by the interplay of this ion-sputtering roughening with the smoothing mechanism of surface diffusion. In particular, these patterns consist of coherent ripples, checkerboard arrays of pits, and periodic distributions of islands or holes when that ion bombardment is at normal incidence. Specifically, nanoscale elevated islands (quantum dots) arranged in close-packed distributions have been experimentally etched on the surface of the semiconductor gallium antimonide [Facsko et al. 1999] or relatively uniform arrays of holes (vacancies), on that of the metal platinum [Michely and Comsa 1991], both by normal-incidence argon ion bombardment. Further, upon examination of the experimental reference [Rusponi et al. 1999] one sees that the normal-incidence neon ion-sputtered erosion patterns occurring on their silver metallic surfaces consisted of either a square checkerboard of pits or a ripple structure of elongated ridges and channels. Finally, in [Rusponi et al. 1997; 1998] which dealt with the argon ion-sputtering of silver and copper surfaces, respectively, these authors also reported coherent ripple formation after normal-incidence bombardment. Such a transition to coherent ripples occurred from a smooth morphology as substrate temperature decreased through a critical value [Rusponi et al. 1997].

In order to model this process, consider a thin solid film of dimensional thickness  $H(r_1, r_2, \tau)$  undergoing normal-incidence ion-bombardment induced erosion, where  $(r_1, r_2)$  represents a transverse laboratory Cartesian coordinate system and  $\tau$  is time. A number of theoretical models have been developed to study the evolution of periodic roughening-type instabilities from coherent ripples to regular arrays of islands or holes in such instances by numerical simulations. These models were derived from conservation of mass at the interfacial solid surface and had as their point of departure the general continuity equation [Makeev et al. 2002]

$$H_{\tau} + K \nabla_{2}^{4} H + \nu_{1} H_{r_{1}r_{1}} + \nu_{2} H_{r_{2}r_{2}} + D_{1} H_{r_{1}r_{1}r_{1}} + D_{2} H_{r_{2}r_{2}r_{2}r_{2}} + D_{12} H_{r_{1}r_{1}r_{2}r_{2}} + J_{0} Y_{0}(H)$$

$$= \frac{1}{2} (\lambda_{1} H_{r_{1}}^{2} + \lambda_{2} H_{r_{2}}^{2}) + H_{r_{1}} (\gamma_{1} + \xi_{1} H_{r_{1}r_{1}} + \xi_{2} H_{r_{2}r_{2}}) + \Omega_{1} H_{r_{1}r_{1}r_{1}} + \Omega_{2} H_{r_{1}r_{2}r_{2}} + \eta_{0}.$$

Here K denotes the thermal surface diffusion coefficient,  $J_0$  the deterministic component of the ion flux,  $Y_0(H)$  the sputtering yield,  $\eta_0$  a noise term resulting from the stochastic component of the ion flux,  $\nabla_2 \equiv (\partial/\partial r_1, \partial/\partial r_2)$ ,  $\nabla_2^2 \equiv \nabla_2 \cdot \nabla_2$ , and  $\nabla_2^4 \equiv (\nabla_2^2)^2$ , while, for the special case of normal-incidence ion bombardment when the impact angle  $\vartheta$  is 0,

$$\gamma_1 = \xi_1 = \xi_2 = \Omega_1 = \Omega_2 = 0,$$
 $\nu_1 = \nu_2 = \nu,$ 
 $D_1 = D_2 = \frac{1}{2}D_{12} = D_0,$ 
 $\lambda_1 = \lambda_2 = \lambda_0,$ 

which converts this equation into its isotropic Kuramoto–Sivashinsky form [Kuramoto 1978; Sivashinsky 1977]

$$H_{\tau} + \nu \nabla_2^2 H + D \nabla_2^4 H + J_0 Y_0(H) = \frac{1}{2} \lambda_0 |\nabla_2 H|^2 + \eta_0,$$

where the effective surface diffusion coefficient satisfies  $D = K + D_0$  and  $|\nabla_2 H|^2 = H_{r_1}^2 + H_{r_2}^2$ .

Then, selecting  $\ell_0 = (2D/\nu)^{1/2}$  and  $\tau_0 = 8D/\nu^2$  as scale factors for length and time, respectively, introducing the dimensionless variables [Wollkind and Vislocky 1990]

$$(x, y) = \frac{(r_1, r_2)}{\ell_0}, \quad t = \frac{\tau}{\tau_0}, \quad h = \frac{H - H_0 + w_n \tau}{\ell_0}, \quad \text{where } w_n = J_0 h_0 \ell_0^2,$$

adopting the sputtering yield relation, consistent with that of [Makeev and Barabási 1998],

$$Y_0(H) = h_0 \ell_0^2 \left[ 1 + \left( \frac{h_0}{\ell_0} \right) \sinh(2h) \right]$$

$$\Rightarrow J_0 Y_0(H) = w_n \left[ 1 + \left( \frac{h_0}{\ell_0} \right) \sinh(2h) \right] = w_0(h),$$

employing the magnitude of the gradient approximation [Siegmann and Rubenfeld 1975]

$$|\nabla_2 H| \cong \frac{\Delta H}{\Delta r} = \frac{|H - (H_0 - w_n \tau)|}{\ell_0} = |h| = \sqrt{h^2},$$

so that its source term will ultimately be of a modified Swift-Hohenberg form [1977] in order to simplify our subsequent analyses [Wollkind et al. 2008], and,

after [Kahng et al. 2001], taking

$$\eta_0 \equiv 0$$
,

we obtain our original damped Kuramoto-Sivashinsky-type equation from this isotropic form

$$h_t + 4\nabla^2 h + 2\nabla^4 h + \beta[\sinh(2h) - \alpha h^2] = 0,$$

where

$$\alpha = \frac{\lambda_0 \ell_0}{2w_n h_0} = \frac{\lambda_0}{2J_0 \ell_0 h_0^2} \in \mathbb{R}, \quad \beta = \frac{\tau_0 w_n h_0}{\ell_0^2} = \tau_0 J_0 h_0^2 = \frac{8DJ_0 h_0^2}{v^2} > 0.$$

Finally, retention of terms through third order in sinh(2h) again yields a modified Swift–Hohenberg truncation of that equation (reviewed in [Cross and Hohenberg 1993])

$$h_t + 4\nabla^2 h + 2\nabla^4 h + \beta (2h - \alpha h^2 + \frac{4}{3}h^3) = 0.$$

Here  $h \equiv$  the nondimensional deviation of the interface from its dimensional mean planar position given by  $H_0 - w_n \tau_0 t$ , where  $w_n \equiv$  the normal velocity of erosion and  $H_0 \equiv$  the initial dimensional uniform thickness of the solid layer,  $h_0 \equiv$  the dimensional maximal interfacial deviation from that mean position,  $\nu \equiv$  the absolute value of the coefficient of negative capillarity,  $\nabla \equiv (\partial/\partial x, \partial/\partial y), \nabla^2 \equiv \nabla \cdot \nabla$ , and  $\nabla^4 \equiv (\nabla^2)^2$ . We shall view  $\alpha$  and  $\beta$  as the nondimensional versions of  $\lambda_0$ , the tilt-dependent coefficient of the erosion rate, and of  $DJ_0$ , respectively. Hence  $\beta$ , which will serve as the bifurcation parameter for our analyses, is a measure of this damping effect to that sputtering pattern formation process caused by the interaction between these two smoothing mechanisms of effective surface diffusion and deterministic ion bombardment. This is the spatiotemporal model evolution equation we wish to analyze for the interfacial morphologies described earlier by performing one-dimensional longitudinal and two-dimensional rhombic planform weakly nonlinear stability analyses of the zero or planar interface solution to that equation. Toward this end, we note that our evolution equation admits this trivial solution  $h \equiv 0$  which satisfies the far-field boundary condition

h remains bounded as 
$$x^2 + y^2 \rightarrow \infty$$

implicitly and represents a planar layer of uniform dimensional thickness  $H = H_0 - w_n \tau$ . In order to compare these theoretical predictions with experimental observations and numerical simulations, it will be necessary for us to introduce the concept of lower- and higher-threshold rhombic patterns based upon the mean position of the interface, which was a paradigm originally employed in [Cangelosi et al. 2015] in relation to ecological Turing pattern formation based upon the population density of mussels in young beds.

# 2. Longitudinal planform weakly nonlinear stability analysis

We first perform a one-dimensional stability analysis of our evolution equation by considering a longitudinal planform solution to it through third-order terms of the form [Davis et al. 2018]

$$h(x, y, t) \sim A_1(t) \cos(qx) + A_1^2(t)[h_{20} + h_{22} \cos(2qx)] + A_1^3(t)[h_{31} \cos(qx) + h_{33} \cos(3qx)],$$

where the amplitude function  $A_1(t)$  satisfies the nonlinear Landau equation [1944]

$$\frac{dA_1}{dt} \sim \sigma A_1 - a_1 A_1^3,$$

 $q \equiv 2\pi/\lambda$ , with  $\lambda \equiv$  wavelength of the class of spatially periodic perturbations under investigation,  $\sigma \equiv$  linear growth rate, and  $a_1 \equiv$  longitudinal planform Landau coefficient. Then substituting this solution into our evolution equation we obtain a problem for each of the terms appearing in that expansion. In particular the linear problem, proportional to  $A_1(t)\cos(qx)$ , yields the secular equation [Schmidt and Kolden 2020]

$$\sigma = 2[\beta_0(q^2) - \beta], \text{ with } \beta_0(q^2) = q^2(2 - q^2).$$

Thus the parabola  $\beta=\beta_0(q^2)$  serves as its marginal stability curve in the  $(q^2,\beta)$ -plane of Figure 1. As can be seen from that figure the maximum value of this parabola occurs at its vertex  $(q_c^2,\beta_c)$ , where  $q_c^2=1$  and  $\beta_c=\beta_0(q_c^2)=1$ . Hence for  $\beta>\beta_c=1$  there exists no  $q^2$  associated with growing modes, while for  $0<\beta<\beta_c$  there exists a band of such wavenumbers squared centered about  $q^2=q_c^2$ . Therefore, the trivial solution is linearly stable for  $\beta>1$ , neutrally stable for  $\beta=1$ , and unstable for  $0<\beta<1$ . Given this linear stability behavior, we, as is usual in such analyses, equate the q and  $\sigma$  in our expansion to  $q=q_c=1$  and  $\sigma=\sigma_0(\beta)=2(1-\beta)$ .

Continuing with our description of the results of this one-dimensional expansion, the second-order problems can be solved in a straightforward manner to yield [Schmidt and Kolden 2020]

$$h_{20}(\beta; \alpha) = \frac{\alpha\beta}{4(2-\beta)}, \quad h_{22}(\beta; \alpha) = \frac{\alpha\beta}{4(10-\beta)}.$$

Although there are also two third-order problems we need only consider the one proportional to  $A_1^3(t)\cos(x)$  containing the Landau coefficient  $a_1$  [Schmidt and Kolden 2020]

$$a_1(\alpha) - 2\sigma_0(\beta)h_{31}(\beta; \alpha) = \beta[1 - \alpha\{2h_{20}(\beta; \alpha) + h_{22}(\beta; \alpha)\}]$$

for our Fredholm alternative method of solvability. Then employing our previous results, taking the limit as  $\beta \to \beta_c = 1$  of this equation, and assuming the requisite

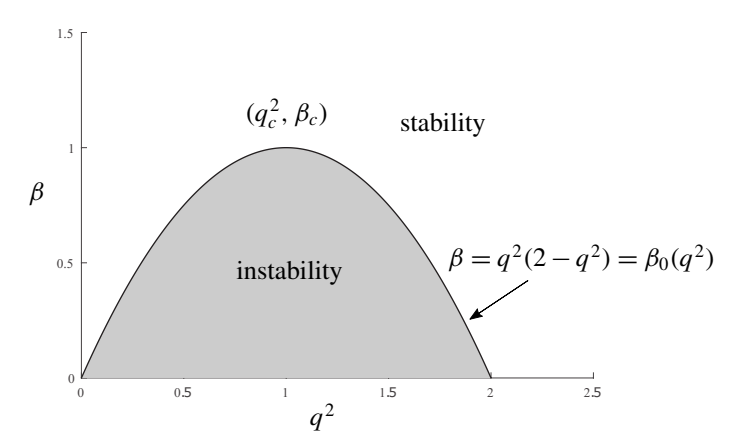


**Figure 1.** Plot of the parabolic marginal stability curve  $\beta = \beta_0(q^2)$  in the  $(q^2, \beta)$ -plane denoting linear behavior.

continuity of  $h_{31}$  at  $\beta = \beta_c$ , we obtain the solvability condition for the longitudinal planform Landau coefficient

$$a_1(\alpha) = 1 - \frac{19}{36}\alpha^2,$$

which then yields the solution

$$h_{31}(\beta;\alpha) = \frac{1}{4} - \frac{\alpha^2}{8} \left( \frac{\beta+2}{2-\beta} + \frac{1}{18} \frac{9\beta+10}{10-\beta} \right).$$

The stability behavior of the Landau amplitude equation and thus the pattern-formation aspect of our damped Kuramoto–Sivashinsky model is crucially dependent upon the sign of  $a_1(\alpha)$ . Hence in order to determine that behavior we must examine this Landau coefficient as a function of  $\alpha$ .

Toward that end, we plot  $a_1(\alpha)$  versus  $\alpha$  in Figure 2. From this figure we see that  $a_1$  has two zeroes at  $\alpha = \alpha_{1,2}$  such that

$$a_1 > 0$$
 for  $\alpha_1 < \alpha < \alpha_2$ ,  $a_1 < 0$  for  $\alpha < \alpha_1$  or  $\alpha > \alpha_2$ ,

where

$$\alpha_{2,1} = \pm \frac{6}{\sqrt{19}} = \pm 1.376.$$

Given these formulae for  $\sigma_0(\beta)$  and  $a_1(\alpha)$ , we note that the Landau amplitude function  $A_1(t)$  undergoes a pitchfork bifurcation [Walgraef 1997] at  $\beta = \beta_c = 1$  when  $\alpha_1 < \alpha < \alpha_2$  from which it may be concluded that [Davis et al. 2018]:

(1) For  $\beta > \beta_c = 1$  and  $\alpha_1 < \alpha < \alpha_2$  ( $\sigma_0 < 0$ ,  $a_1 > 0$ ), the planar or smooth interface solution  $h \equiv 0$  is stable to both infinitesimal and one-dimensional finite amplitude disturbances. Since  $\sigma_0 < 0$ , linear theory predicts stability of the undisturbed state  $A_1 \equiv 0$  and our nonlinear effects enhance this stabilizing behavior.

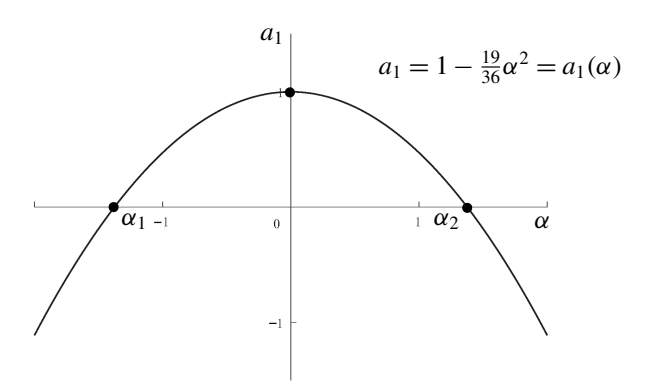


**Figure 2.** Plot of the parabolic formula for the longitudinal planform Landau coefficient  $a_1$  versus  $\alpha$ .

(2) For  $0 < \beta < \beta_c = 1$  and  $\alpha_1 < \alpha < \alpha_2$  ( $\sigma_0$ ,  $a_1 > 0$ ), there exists a stable equilibrium solution  $A_e^2 = \sigma_0/a_1$ . Since  $\sigma_0 > 0$ , linear theory would predict instability, whereas our nonlinear analysis shows the existence of this finite amplitude supercritically stable equilibrium state. Specifically that stable equilibrium point corresponds to a steady-state re-equilibrated spatially nonuniform pattern given by

$$\lim_{t \to \infty} h(x, y, t) = h_e(x) = \delta \cos\left(\frac{2\pi x}{\lambda_c}\right) + O(\delta^2), \quad -\infty < x < \infty,$$

where

$$\delta = A_e + h_{31}(1; \alpha) A_e^3 > 0$$
, with  $h_{31}(1; \alpha) = \frac{1}{4} - \frac{1}{8}\alpha^2 (3 + \frac{19}{162})$ ,

which represents a periodic one-dimensional interfacial morphology consisting of coherent stationary parallel ripples (it might seem more logical to use the term ridges for such patterns but here we have adopted the standard terminology employed for them), having a characteristic wavelength of

$$\lambda_c = \frac{2\pi}{q_c} = 2\pi, \quad \lambda_c^* = \ell_0 \lambda_c = 2\pi \ell_0 = 2\pi \left(\frac{2D}{\nu}\right)^{1/2},$$

in dimensionless and dimensional variables, respectively, the latter quantity being generated by the competition between surface tension  $(\nu)$  and effective surface diffusion (D). These supercritical ripples are represented in the contour plot of Figure 3, where the axes are being measured in units of  $\lambda_c$ , while consistent with both experimental observation and numerical simulation, elevations (h > 0) from the original mean position of the interface (h = 0) appear light and depressions (h < 0), dark. In our rhombic planform analysis of the next section we shall label such a protocol as a zero-threshold pattern.

When  $\alpha < \alpha_1$  or  $\alpha > \alpha_2$ , this bifurcation is subcritical. The implications of such subcriticality have recently been described in detail in [Davis et al. 2018]. In what

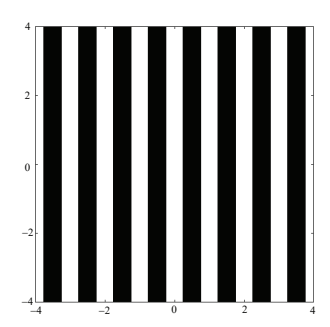


**Figure 3.** Contour plot in the (x, y)-plane for coherent ripples (critical point II of the rhombic planform stability analysis), where the spatial variables are measured in units of  $\lambda_c$ . Here elevations appear light and depressions, dark, in accordance with experimental observation. This transition occurs at h = 0, which is a protocol that will be labeled zero threshold for our rhombic planform stability analysis. We shall show from this analysis that coherent ripples are only stable where a protocol of the zero threshold type holds. Hence this contour plot is the representation for critical point II as identified in the  $(\alpha, \beta)$ -plane of the morphological stability diagram of Figure 7.

follows we shall be concentrating on the behavior of our model in its supercritical regime where  $\alpha_1 < \alpha < \alpha_2$ .

# 3. Rhombic planform weakly nonlinear stability analysis

In order to refine these one-dimensional predictions we investigate two-dimensional ion-sputtered erosion patterns by seeking a rhombic planform solution of our damped Kuramoto–Sivashinsky type equation which, to lowest order, can be written as [Wollkind et al. 1994]

$$h(x, y, t) \sim A_1(t)\cos(x) + B_1(t)\cos(z)$$
, with  $z = x\cos(\varphi) + y\sin(\varphi)$ ,

where  $A_1(t)$ ,  $B_1(t)$  satisfy the nonlinear system of amplitude equations

$$\frac{dA_1}{dt} \sim \sigma A_1 - A_1(a_1 A_1^2 + b_1 B_1^2) = F(A_1, B_1),$$

$$\frac{dB_1}{dt} \sim \sigma B_1 - B_1(b_1 A_1^2 + a_1 B_1^2) = G(A_1, B_1),$$

 $\varphi \in \left(0, \frac{\pi}{2}\right] \equiv$  the rhombic angle,  $b_1 \equiv$  rhombic planform Landau coefficient, and each higher-order term in that expansion is of the form

$$h_{ijnk}A_1^i(t)B_1^j(t)\cos(nx+kz).$$

Then substituting this expansion into our damped Kuramoto–Sivashinsky-type model equation, we obtain a sequence of problems, each of which is proportional to one of these terms. Solving those problems, we find that [Schmidt and Kolden 2020]

$$h_{i0n0} = h_{0i0n} = h_{in}$$
,  $\sigma = \sigma_0(\beta) = 2(\beta - 1)$ ,  $a_1 = a_1(\alpha) = 1 - \frac{19}{36}\alpha^2$ ,

as defined in Section 2, while

$$h_{111(\pm 1)}(\beta; \alpha, \varphi) = \frac{\alpha}{2} \frac{\beta}{2 - \beta + 4\cos(\varphi)[\cos(\varphi) \pm 1]}$$

and  $b_1$ , in particular, satisfies

$$b_1(\alpha, \varphi) - 2\sigma_0(\beta)h_{2101}(\beta; \alpha, \varphi) = \beta[2 - \alpha\{2h_{2000} + h_{1111} + h_{111(-1)}\}(\beta; \alpha, \varphi)].$$

Now taking the limit of this equation as  $\beta \to 1$  and making use of our previous results, we obtain the solvability condition for the rhombic planform Landau coefficient

$$b_1(\alpha, \varphi) = 2 - \frac{\alpha^2}{2} \frac{3 + 16\cos^4(\varphi)}{[4\cos^2(\varphi) - 1]^2}.$$

Having developed these formulae for its growth rate and Landau coefficients, we turn our attention to the rhombic planform amplitude equations which possess the equivalence classes of critical points  $(A_0, B_0)$  such that  $F(A_0, B_0) = G(A_0, B_0) = 0$  with  $A_0, B_0 \ge 0$  given by

I: 
$$A_0 = B_0 = 0$$
,  
II:  $A_0^2 = \frac{\sigma}{a_1}$ ,  $B_0 = 0$ ,  
V:  $A_0 = B_0$ , with  $A_0^2 = \frac{\sigma}{a_1 + b_1}$ .

Here, since we are considering  $\alpha_1 < \alpha < \alpha_2$ ,  $a_1 > 0$  and it is assumed that  $a_1 + b_1 > 0$  as well. Hence critical points II and V will only occur provided  $\sigma > 0$  or  $0 < \beta < 1$ . We now examine the orbital stability of these critical points where by orbital stability of pattern formation is meant a family of solutions in the plane that may interchange with each other but do not grow or decay into a solution type from a different family [Kuske and Matkowsky 1994]. Such an interpretation in nonlinear stability theory depends upon the symmetries inherent to the form of the particular planform solution, these invariances also limiting each equivalence class of critical points to a single member that must be considered explicitly when examining their stability. We investigate that stability by first seeking a solution of our rhombic planform amplitude equations of the form

$$A_1(t) = A_0 + \varepsilon A(t) + O(\varepsilon^2), \quad B_1(t) = B_0 + \varepsilon B(t) + O(\varepsilon^2), \quad \text{with } |\varepsilon| \ll 1,$$

and, employing Taylor series of functions of two variables for  $F(A_1, B_1)$  and  $G(A_1, B_1)$  about  $(A_0, B_0)$ , show that the perturbation quantities A(t), B(t), upon neglect of terms of  $O(\varepsilon^2)$  and cancellation of the  $\varepsilon$ -factor, satisfy the linear homogeneous ordinary differential equation system

$$\frac{d\mathcal{A}}{dt} = c_{11}\mathcal{A} + c_{12}\mathcal{B}, \quad \frac{d\mathcal{B}}{dt} = c_{21}\mathcal{A} + c_{22}\mathcal{B},$$

where

$$c_{11} = \frac{\partial F}{\partial A_1}(A_0, B_0) = \sigma - 3a_1 A_0^2 - b_1 B_0^2,$$

$$c_{12} = \frac{\partial F}{\partial B_1}(A_0, B_0) = c_{21} = \frac{\partial G}{\partial A_1}(A_0, B_0) = -2b_1 A_0 B_0,$$

$$c_{22} = \frac{\partial G}{\partial B_1}(A_0, B_0) = \sigma - 3a_1 B_0^2 - b_1 A_0^2.$$

Then letting  $[A, B](t) = [C_1, C_2]e^{pt}$ , where  $C_1^2 + C_2^2 \neq 0$ , we obtain, after cancellation of the  $e^{pt}$ -factor, the linear homogeneous system of algebraic equations for the constants  $C_1$  and  $C_2$ 

$$(p-c_{11})\mathcal{C}_1 - c_{12}\mathcal{C}_2 = 0, \quad -c_{21}\mathcal{C}_1 + (p-c_{22})\mathcal{C}_2 = 0,$$

which, upon imposition of the vanishing of the determinant of the matrix of its coefficients to guarantee the nontriviality property for these constants, yields the following quadratic in *p*:

$$(p - c_{11})(p - c_{22}) - c_{12}^2 = 0.$$

Now, particularizing this quadratic to the specific  $(A_0, B_0)$ -values of the critical points and noting that under these conditions it has the associated roots  $p_1 = c_{11} + c_{12}$  and  $p_2 = c_{22} - c_{12}$  since either  $c_{12} = 0$  for I and II or  $c_{11} = c_{22}$  for V, we conclude that

I: 
$$p_{1,2} = \sigma$$
,  
II:  $p_1 = -2\sigma$ ,  $p_2 = \frac{(a_1 - b_1)\sigma}{a_1}$ ,  
V:  $p_1 = -2\sigma$ ,  $p_2 = \frac{2(b_1 - a_1)\sigma}{a_1 + b_1}$ .

Finally, requiring  $p_{1,2} < 0$ , we deduce the stability criteria:

I is stable for 
$$\sigma < 0$$
,  
II is stable for  $\sigma > 0$ ,  $b_1 > a_1$ ,  
V is stable for  $\sigma > 0$ ,  $a_1 > b_1$ .

Observe that since those criteria are mutually exclusive there can never be pairwise bistability between these critical points. Also note that  $\sigma > 0$  is both an existence

condition and a stability criterion for critical points II and V (the II equivalence class also contains  $A_0 = 0$ ,  $B_0^2 = \sigma/a_1$ ).

Before examining the implications of those stability criteria, we make a morphological interpretation of the potentially stable critical points relative to the ion-sputtered erosion patterns under investigation. Then to lowest order the interfacial deviation associated with these critical points is given by

$$\lim_{t \to \infty} h(x, y, t) = h_e(x, y) \sim A_0 \cos(x) + B_0 \cos(z), \quad \text{where } z = x \cos(\varphi) + y \sin(\varphi).$$

Thus, critical points I and II correspond to the smooth planar surface and coherent ripples, respectively, already discussed in the longitudinal planform analysis. To make an analogous interpretation of critical point V, we consider this deviation function with  $A_0 = B_0 > 0$  and introduce the concept of lower, zero, and higher threshold patterns based upon the mean position of the interface. To do so we must first examine how what in fluid mechanics are called the mean motion terms [Segel 1966] from our nonlinear stability analysis have altered that interfacial position. These homogeneous higher-order terms in  $h_e(x, y)$  for critical point V are given by

$$h_{2000}A_0^2 + h_{0200}B_0^2$$
 with  $A_0 = B_0$  or  $2h_{20}B_0^2$ 

since

$$h_{2000} = h_{0200} = h_{20} = \frac{\alpha \beta}{4(2-\beta)}.$$

Then, adding these terms to the original dimensional mean position of the interface and employing our previous results, we find that this mean position to second-order now satisfies

$$H_m = H_0 - w_n \tau + \frac{\alpha \beta \ell_0 B_0^2}{2(2-\beta)}.$$

We next adopt the protocol that in our contour plots of critical point V the elevations, which satisfy  $H > H_m$ , will appear light, and depressions, which satisfy  $H < H_m$ , dark, while  $H = H_m$  or  $h = 2h_{20}B_0^2$  represents the threshold value at which this transition occurs. When  $h_{20}$  is less than, equal to, or greater than zero we shall label such patterns as being of lower, zero, or higher threshold, respectively. Hence to determine the proper threshold type we must examine the sign of  $h_{20}$ . Rewriting this quantity as  $h_{20} = \gamma/[4(2-\beta)]$ , where  $\gamma = \alpha\beta = \tau_0\lambda_0/(2\ell_0)$  and recalling that for stable rhombic patterns  $\sigma = \sigma_0(\beta) = 2(1-\beta) > 0$ , we can conclude that this behavior of  $h_{20}$  depends on the sign of  $\lambda_0$ , which, being the tilt-dependent coefficient of the erosion rate, is a real-valued parameter with the dimension of velocity. Therefore our stable rhombic patterns will be of lower, zero, or higher threshold type depending upon whether  $\lambda_0 < 0$ ,  $\lambda_0 = 0$ , or  $\lambda_0 > 0$ , respectively. To make a physical interpretation of these results we note that to lowest order the

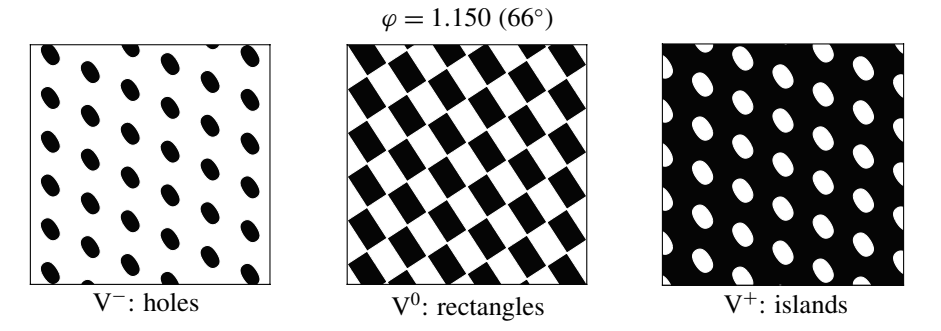


**Figure 4.** Rhombic patterns in the (x, y)-plane relevant to g(x, z) for  $\varphi = 1.150$  (66°) with threshold values from left to right of -1, 0, and 1, which are denoted by  $V^-$ ,  $V^0$ , and  $V^+$ , respectively, and represent arrays of holes, rectangles, and islands. Here, the spatial variables are being measured in units of  $\lambda_c$  with regions below that threshold in each part appearing dark and regions above it, light. Note that  $|g(x,z)| \le 2$  and  $\varphi = 1.150$  is a typical allowable angle for  $\alpha = 0.447$  which corresponds to the value of that parameter for the experiments of [Facsko et al. 1999]. Observe that for this angle the  $V^{\pm}$  patterns approximate the close-packed structure of hexagonal arrays.

equilibrium erosion pattern associated with critical point V satisfies

$$h_e(x, y) \sim B_0 g(x, z)$$
 for  $z = x \cos(\varphi) + y \sin(\varphi)$  and  $B_0 > 0$ ,

where

$$g(x, z) = \cos\left(\frac{2\pi x}{\lambda_c}\right) + \cos\left(\frac{2\pi z}{\lambda_c}\right).$$

The three parts of Figure 4 are threshold contour plots of g(x, z) for the typical rhombic angle (see below)  $\varphi = 1.150~(66^{\circ})$  with the threshold values of -1, 0, and 1, respectively. Here, the spatial variables are being measured in units of  $\lambda_c$  with regions exceeding that threshold in each part appearing light and regions less than it, dark. Given their appearance in Figure 4 we shall identify these lower, zero, and higher threshold-type rhombic arrays with erosion patterns of holes, rectangles, and islands, respectively, denoting them by  $V^-$ ,  $V^0$ , and  $V^+$  in what follows. We repeat this process and obtain the threshold contour plots of g(x,z) for  $\varphi = \frac{\pi}{2}~(90^{\circ})$  or z = y which appear in Figure 5. From the checkerboard structure of these arrays it is clear that this state should be identified with an ion-sputtered erosion pattern of square planform.

Having completed these morphological identifications, we are ready to examine the existence and stability of critical points II and V. Toward that end we determine the signs of  $a_1 \pm b_1$  for  $\alpha \in \mathbb{R}$  and  $0 < \varphi \le \frac{\pi}{2}$ . To illustrate this procedure, consider

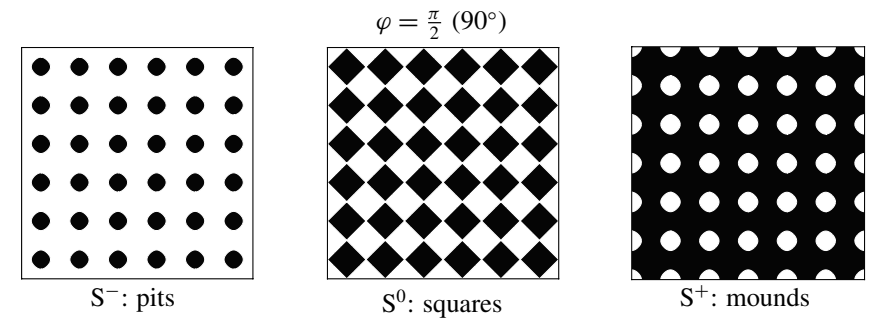


**Figure 5.** Square patterns relevant to g(x, y) for  $\varphi = \frac{\pi}{2}$  (90°) with threshold values from left to right of -1, 0, and 1, which are denoted by S<sup>-</sup>, S<sup>0</sup>, and S<sup>+</sup>, respectively, and represent arrays of pits, squares, and mounds. Here, the spatial variables are again being measured in units of  $\lambda_c$  with regions below that threshold in each part appearing dark and regions above it, light. In particular, contrast the appearance of these patterns with the corresponding ones from Figure 4. Sekimura et al. [1999] referred to S<sup>±</sup> collectively as "square spots" in their lepidoptera wing pattern formation square-type planform nonlinear stability analysis to distinguish them from hexagonal arrays of spots. In hexagonal planform nonlinear stability analyses such structures are often denoted by III<sup>±</sup> while its generalized cell which is always unstable is denoted by IV; hence, our choice of the notation V for the rhombic critical point [Wollkind and Dichone 2017].

the existence and stability of the square planform obtained by setting  $\varphi = \frac{\pi}{2}$  for critical point V. Given that

$$a_1(\alpha) + b_1(\alpha, \frac{\pi}{2}) = 3 - \frac{73}{36}\alpha^2 > 0$$
 whenever  $\alpha^2 < \frac{108}{73}$ , 
$$b_1(\alpha, \frac{\pi}{2}) = 2 - \frac{3\alpha^2}{2} < 1 - \frac{19}{36}\alpha^2 = a_1(\alpha)$$
 whenever  $\alpha^2 > \frac{36}{35}$ ,

both are valid whenever  $\frac{36}{35} < \alpha^2 < \frac{108}{73}$ . Hence we can conclude that square rhombic patterns would be stable versus ripples for

$$1.014 = \frac{6}{\sqrt{35}} < |\alpha| < \sqrt{\frac{108}{73}} = 1.216$$
 provided  $\sigma > 0$  or  $0 < \beta < 1$ .

Then we investigate this behavior for fixed values of  $\alpha$  and, since our Landau coefficients are symmetric in that parameter, we need only consider  $\alpha \geq 0$ . Observe in this context that

$$b_1(0, \varphi) = 2 > 1 = a_1(0)$$

and thus, for  $\alpha=0$  and  $0<\beta<1$ , ripples are stable versus rhombic patterns. We find that for  $0<\alpha<\sqrt{\frac{108}{73}}$  there exist two  $\varphi$ -intervals  $(\varphi_m,\varphi_M)$  and  $(\varphi_\ell,\varphi_r)$ ,

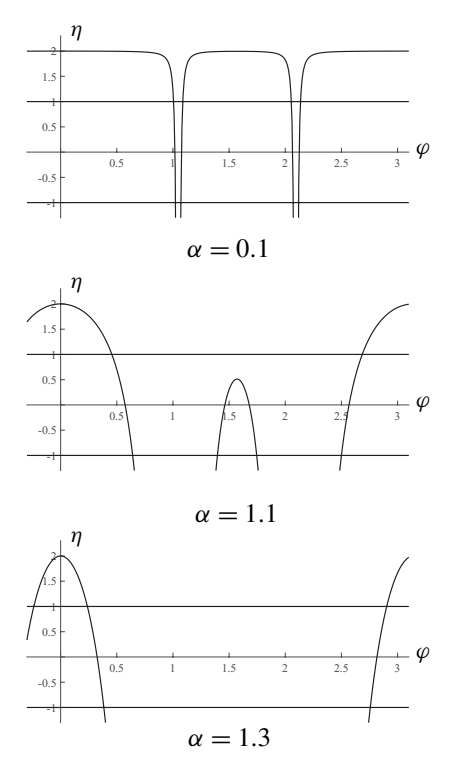


**Figure 6.** Plots of  $\eta$  versus  $\varphi$  for  $\alpha = 0.1$ ,  $\alpha = 1.1$ , and  $\alpha = 1.3$ . Here the  $\varphi$ -intervals where  $-1 < \eta < 1$  correspond to stable rhombic patterns and appear in Table 1 for those  $\alpha$ -values. Note that  $\eta$  has been plotted for  $0 < \varphi < \pi$  to demonstrate the symmetry of that function about  $\varphi = \frac{\pi}{2}$ .

flanking  $\varphi = \frac{\pi}{3}$ , in which  $a_1(\alpha) \pm b_1(\alpha, \varphi) > 0$ , or equivalently  $-1 < \eta(\alpha, \varphi) = b_1(\alpha, \varphi)/a_1(\alpha) < 1$ , where

$$0 < \varphi_m(\alpha) < \varphi_M(\alpha) < \frac{\pi}{3} < \varphi_\ell(\alpha) < \varphi_r(\alpha) \le \frac{\pi}{2}$$

and thus, rhombic patterns of these characteristic angles are stable versus ripples, while for  $\sqrt{\frac{108}{73}} < \alpha < \frac{6}{\sqrt{19}}$  only the  $(\varphi_m, \varphi_M)$  interval exists (see Figure 6). These values are tabulated in Table 1. Note that although this limit exists such an occurrence implies

$$\lim_{\alpha \to 0} b_1(\alpha, \varphi) \neq b_1(0, \varphi)$$

or  $b_1(\alpha, \varphi)$  has a jump discontinuity at  $\alpha = 0$ , something conclusively demonstrated for their rhombic-planform nonlinear stability analysis in [Cangelosi et al. 2015]. Note the refinement of our longitudinal planform stability results when  $0 < \beta < 1$  provided by these rhombic planform predictions is that stable ripples (II) will only

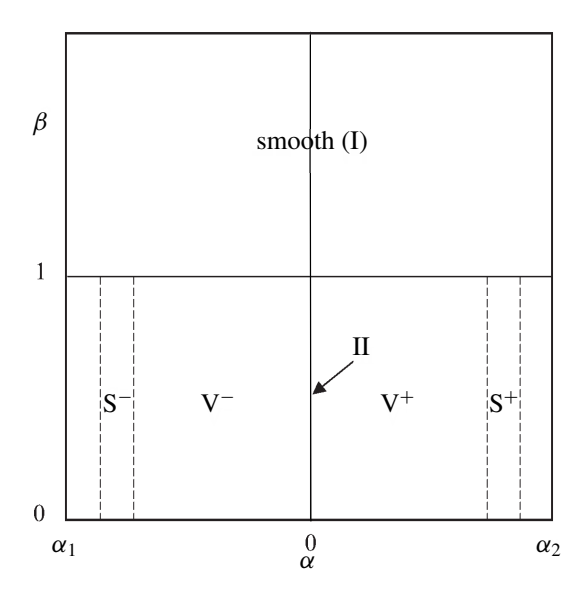


**Figure 7.** Morphological nonlinear stability diagram in the  $(\alpha, \beta)$ plane for our damped Kuramoto-Sivashinsky type equation identifying the predicted ion-sputtered erosion patterns. Here the regions between the dotted lines indicate parameter ranges where stable rhombic patterns  $(V^{\pm})$  of angle  $\varphi = \frac{\pi}{2}$  or squares  $(S^{\pm})$  can occur while the region of stable ripples associated with critical point II is identified by an arrow. Observe that the other member of this equivalence class denoted in the text by  $A_0 = 0$ ,  $B_0^2 = \sigma/a_1$  gives rise to roots which simply interchange the values of  $p_1$  and  $p_2$  for the member chosen to represent that equivalence class and in so doing preserves our stability criteria for this class while rotating its deviation function now satisfying  $h_e(z) \sim \delta \cos(2\pi z/\lambda_c)$  through an angle  $\varphi$ , when compared to the contour plot of Figure 3, characteristic of the rotational invariances of such orbital stabilities. Thus, given the isotropic nature of our model evolution equation defined on an unbounded domain, there is no preferred direction and hence both these families of stripes are equally likely to occur [Sekimura et al. 1999] with arbitrary initial conditions determining which of those orientations is actually selected [Segel 1966]; e.g., if  $\varphi = \frac{\pi}{2}$  were selected the vertical stripes of Figure 3 would be replaced by horizontal ones instead.

occur for  $\alpha=0$  or equivalently  $\lambda_0=0$ , while, for  $0<\alpha<\alpha_2=\frac{6}{\sqrt{19}}$  ( $\lambda_0>0$ ), islands  $(V^+)$  of the allowable characteristic angles are the only stable patterns and, for  $-\frac{6}{\sqrt{19}}=\alpha_1<\alpha<0$  ( $\lambda_0<0$ ), holes  $(V^-)$  of these characteristic angles are the only stable patterns. In addition, square patterns  $(S^\pm)$  of rhombic angle  $\varphi=\frac{\pi}{2}$  can

α	$\varphi_m$	$\varphi_M$	$arphi_\ell$	$\varphi_r$
0.1	1.006	1.023	1.071	1.088
0.2	0.963	0.999	1.094	1.127
0.3	0.919	0.974	1.118	1.167
0.4	0.873	0.947	1.142	1.206
0.5	0.826	0.918	1.167	1.245
0.6	0.775	0.887	1.194	1.286
0.7	0.722	0.853	1.223	1.329
0.8	0.664	0.813	1.255	1.376
0.9	0.602	0.768	1.292	1.432
1.0	0.534	0.712	1.377	1.523
1.1	0.456	0.641	1.396	1.571
1.2	0.363	0.544	1.504	1.571
1.3	0.238	0.385	none	none

**Table 1.** The  $\varphi$ -range for stable rhombic patterns of these characteristic angles versus  $\alpha$ .

only occur for  $1.014 = \frac{6}{\sqrt{35}} < |\alpha| < \sqrt{\frac{108}{73}} = 1.216$ . Observe that for  $\beta > 1$ , both our planforms predict that only the smooth planar surface (I) can occur. These morphological nonlinear stability predictions are represented diagrammatically in the  $(\alpha, \beta)$ -plane of Figure 7.

# 4. Application to ion-sputtered erosion-pattern experimental evidence

We are now ready to compare our two-dimensional ion-sputtered erosion morphological stability predictions summarized in Figure 7 with the normal-incidence experimental observations that were described in Section 1. We begin with the quantum dot island semiconductor experiments of [Facsko et al. 1999]. To compare our theoretical predictions with their results we first have to decide what values to assign the material and experimental parameters appearing in our model equation since some of the relevant quantities were unreported. Given that [Facsko et al. 1999] also produced the same quantum dot island formation on germanium surfaces bombarded with argon ions as they did on gallium antimonide ones, we use parameter values as measured in [Chason et al. 1994] who investigated temperature-dependent erosion during xenon ion sputtering of the group IV semiconductor germanium. Toward that end, we take

$$v = 2 \times 10^{-15} \frac{\text{cm}^2}{\text{sec}},$$

$$D = 0.8 \times 10^{-27} \frac{\text{cm}^4}{\text{sec}},$$

$$h_0 = 0.1 \text{ nm} \quad (\text{nm} \equiv 10^{-9} \text{ m}),$$

where these were appropriate values for normal-incidence ion sputtering at a substrate temperature  $T_S = 423$  K. Then employing those values in the scale factors for length and time, we find that

$$\ell_0 = 8.94 \,\text{nm}, \quad \tau_0 = 1.60 \times 10^3 \,\text{sec}.$$

Thus, from the definitions of  $\beta$  and  $w_n$ , we see that  $\beta \cong \beta_c = 1$  with  $\beta < 1$  corresponds to

$$J_0 \cong 6.25 \times 10^{12} \frac{1}{\text{cm}^2 \text{sec}}, \quad w_n \cong 0.50 \frac{\text{nm}}{\text{sec}},$$

which are of the same order of magnitude for these quantities as those in the experiments of [Chason et al. 1994; Facsko et al. 1999], respectively. Finally, we take

$$2\lambda_0 = 0.01 \, \frac{\text{nm}}{\text{sec}},$$

which is the value [Facsko et al. 2004] subsequently employed for this parameter in the numerical simulation of their model ion-sputtering evolution equation. Now recalling the relationship  $\alpha = \tau_0 \lambda_0/(2\ell_0 \beta)$ , we find for these selected values of  $\tau_0$ ,  $\ell_0$ ,  $\lambda_0/2$ , and  $\beta$  that

$$\alpha \cong 0.447$$
.

Upon examination of our rhombic planform morphological stability results contained in Figure 7, we can conclude that such a value of  $0 < \alpha < \alpha_2 = 1.376$  is compatible with a prediction of quantum dot island (V<sup>+</sup>) formation when  $\beta \cong \beta_c = 1$  for  $\beta < 1$ . Further, given the selected value of  $\ell_0$ , we obtain from the definition of the pattern dimensional wavelength  $\lambda_c^*$  that

$$\lambda_c^* = 56.2 \, \text{nm}.$$

Since [Facsko et al. 1999] stated that  $\lambda_c^*$  closely approximated the size of these quantum dot islands as determined by average diameter  $d_c^*$ , this compares quite favorably with their measured experimental value of  $d_c^* = 50 \, \mathrm{nm}$ . Hence our theoretical predictions are in both very good qualitative and quantitative agreement with those quantum dot island experimental observations.

To investigate the origin and dynamics of such quantum dot island formation under normal-incidence ion sputtering, Kahng et al. [2001] numerically integrated a continuum evolution equation for the dimensional deviation of the interfacial surface from its mean planar position  $H_0 - w_n \tau$  that is derivable from the isotropic continuity equation with  $\eta_0 \equiv 0$  upon the implicit adoption of the constant sputtering yield condition

$$J_0Y_0(H) \equiv w_0(0) = w_n$$

instead of our sinh(2h)-dependent one. By necessity these simulations were performed on a square spatial domain with periodic boundary conditions which are the numerical analog of our far-field condition. We note in this context that it seems reasonable as a first approximation for us to have considered our model equation on an unbounded spatial domain since the characteristic transverse length scale of the thin solid films was much greater than the wavelength of the patterns under investigation in these experiments and consequently their actual lateral boundaries did not significantly influence the patterns [Graham et al. 1994]. Specifically, Kahng et al. [2001] performed their numerical simulations on this undamped Kuramoto-Sivashinsky evolution equation for the idealized parameter values  $\lambda_0 = \pm 1$  nm/sec, obtaining a regular lattice of elevated islands when  $\lambda_0 = 1$  nm/sec and a similar lattice of holes when  $\lambda_0 = -1$  nm/sec. Hence, they concluded that their predicted morphologies for  $\lambda_0 > 0$  were reminiscent of the patterns reported in [Facsko et al. 1999]. We note that those for  $\lambda_0 < 0$  closely resembled the uniform distribution of holes which resulted from argon ion-sputtering of platinum under normal incidence in [Michely and Comsa 1991]. Therefore, in light of these theoretical, experimental, and numerical outcomes, we conjecture that  $\lambda_0 > 0$  is to be expected for ionsputtering of semiconductor materials.

Next, we consider the morphological stability predictions of our model relevant to these experimental observations of [Michely and Comsa 1991; Rusponi et al. 1997; 1998; 1999] involving the ion-sputtering of metals. Clearly, the lattice of vacancies produced in [Michely and Comsa 1991] at a substrate temperature  $T_S$  from 550 K to 625 K on a normal-incidence argon-ion sputtered platinum surface when compared with the uniform array of holes (V<sup>-</sup>) predicted in our stability diagram of Figure 7 require  $\alpha_1 < \alpha < 0$  ( $\lambda_0 < 0$ ) and  $0 < \beta < 1$ . They referred to such depressions as vacancy islands to distinguish them from normal islands. Our rhombic planform stability analysis for  $\varphi = \frac{\pi}{2}$  predicted that checkerboard arrays of mounds (S<sup>+</sup>) or pits (S<sup>-</sup>) would require  $0 < \beta < 1$  and  $1.014 = \frac{6}{\sqrt{35}} < |\alpha| < \sqrt{\frac{108}{73}} = 1.216$ . Now making the companion conjecture that  $\lambda_0 \le 0$  is to be expected for ionsputtering of metallic materials, this condition reduces to  $\alpha_1 < -1.216 < \alpha < -1.014$ , which is consistent with the square checkerboard of pits (S<sup>-</sup>) observed in [Rusponi et al. 1999] on a neon ion-sputtered silver surface at normal incidence (note its  $\lambda_c^* = 55$  nm!). Kahng et al. [2001] erroneously claimed that their  $\lambda_0 < 0$  simulations were a theoretical confirmation of this result rather than that of [Michely and Comsa 1991]. Further, from Figure 7 for our rhombic planform morphological stability analysis, we can conclude that the coherent ripples (II) produced by [Rusponi et al. 1997; 1998; 1999] under argon or neon ion-sputtering of silver or copper erosion surfaces at normal incidence require  $\alpha = 0$ , or equivalently  $\lambda_0 = 0$ , since such patterns are only stable at this value of that parameter and when  $0 < \beta < \beta_c = 1$ . Observe for  $\beta > \beta_c = 1$  and  $\alpha = 0$ , the planar or smooth interface solution (I) is the

only stable state. Hence there is an exchange of stabilities for  $\alpha=0$  between these two states at  $\beta=\beta_c=1$ . We employ this result to show that the predictions of our model are compatible with the transition between those states that occurred in the experiments of [Rusponi et al. 1997] upon decreasing the substrate temperature. First recalling from its definition that  $\beta=8J_0h_0^2D/v^2$  and then noting that the thermal diffusion coefficient K satisfies a relationship of the form [Makeev and Barabási 1997]

$$K = K_0 \exp\left(-\frac{T_0}{T_S}\right) = K(T_S),$$

where  $K_0$  and  $T_0$  are positive characteristic values, we derive the following substrate temperature dependence of the effective surface diffusion coefficient:

$$D = K(T_S) + D_0 = D(T_S).$$

Thus, since the other quantities appearing in our formula for  $\beta$  are virtually invariant over the substrate temperature range of interest, incorporation of this function into that formula yields

$$\beta = \frac{8J_0h_0^2D(T_S)}{v^2} = \beta(T_S).$$

Hence, because  $K(T_S)$  increases exponentially with substrate temperature given that

$$K'(T_S) = \left(\frac{T_0}{T_S^2}\right) K(T_S) > 0,$$

we deduce there exists a critical value of this temperature  $T_c$ , defined implicitly by

$$\beta(T_c) = \beta_c = 1$$

such that

$$\beta > \beta_c = 1$$
 for  $T_S > T_c$  and  $\beta < \beta_c = 1$  for  $T_S < T_c$ ,

which serves as a point of transition between the smooth and rippled morphologies along the vertical line  $\alpha = 0$  of Figure 7 when substrate temperature is decreased through it in accordance with the experimental evidence of [Rusponi et al. 1997].

Having demonstrated that given the proper identification of its parameter values our theoretical model predictions agree very well with relevant experimental observation and numerical simulation, we discuss a general symmetry property of the damped Kuramoto–Sivashinsky-type governing equation responsible for this correlation. As pointed out in [Kahng et al. 2001] for their undamped Kuramoto–Sivashinsky equation, the morphological reversal which occurred upon the change in sign of  $\alpha$  could be anticipated from its qualitative behavior. Specifically, our equation is invariant under the simultaneous transformation  $h \to -h$  and  $\alpha \to -\alpha$  by virtue of both  $\sinh(-2h) = -\sinh(2h)$  and  $(-h)^2 = h^2$  which indicates that the

change in sign of  $\alpha$  did not affect its interfacial dynamics but merely turned island patterns into mirror-imaged ones involving holes. This also indicates that such patterns are intrinsically nonlinear since had linear terms alone been responsible for their formation, the surface morphology would not have depended on the sign of  $\alpha$  [Kahng et al. 2001]. This being the case there was some merit for us to examine further its other nonlinear effect, which provided the damping in our equation.

To do so we considered our sputtering yield constitutive relation with  $H = h_0 + H_0 - w_n \tau$  or equivalently  $h = h_0/\ell_0$  in its normalized form

$$\frac{Y_0(h_0 + H_0 - w_n \tau)}{h_0 \ell_0^2} = 1 + \frac{h_0}{\ell_0} \sinh\left(\frac{2h_0}{\ell_0}\right).$$

Then employing the series for sinh through third-order, we obtained the representation

$$1 + \frac{h_0}{\ell_0} \sinh\left(\frac{2h_0}{\ell_0}\right) \sim 1 + 2\left(\frac{h_0}{\ell_0}\right)^2 + \frac{4}{3}\left(\frac{h_0}{\ell_0}\right)^4$$

which is consistent with the asymptotic result of [Makeev and Barabási 1998]

$$C_1 + C_2 h_0^2 + O(h_0^4)$$
, where  $C_1 = 1$  and  $C_2 > 0$ ,

for that normalized yield. Hence, we initially introduced a general secondary yield term in our constitutive relation of the form

$$r(h) = 2h + \mu_0 h^3 + O(h^5)$$

rather than the particular function  $\sinh(2h)$  appearing there. Since that function only contained odd powers of h and thus r(-h) = -r(h), our damped Kuramoto–Sivashinsky-type equation would still exhibit the symmetry property discussed above. Then our longitudinal and rhombic planform weakly nonlinear stability analyses resulted in the Landau coefficients

$$a_1(\alpha; \mu_0) = \frac{3\mu_0}{4} - \frac{19\alpha^2}{36}, \quad b_1(\alpha, \varphi; \mu_0) = \frac{3\mu_0}{2} - \frac{\alpha^2}{2} \frac{3 + 16\cos^4(\varphi)}{[4\cos^2(\varphi) - 1]^2},$$

which, of course, reduced to their previously obtained formulae for  $\mu_0 = \frac{4}{3}$ . Given that the transition between smooth and rippled morphologies with substrate temperature observed in [Rusponi et al. 1997] was nonhysteretical, we moreover assumed  $\mu_0 > 0$  in order to eliminate the possibility of such metastability by guaranteeing

$$b_1 - a_1 = a_1 = \frac{3}{4}\mu_0 > 0$$
 for  $\alpha = 0$ .

Finally, since Makeev and Barabási [1998] did not find any oscillatory behavior for their normalized yield function, we adopted the specific odd nonperiodic

secondary yield term

$$r(h) = \sinh(2h) \implies \mu_0 = \frac{4}{3},$$

this selection having been made for the sake of definiteness as well as being motivated by the form of that interfacial model equation analyzed in [Wollkind and Vislocky 1990], which was also the rationale for our choice of scale factors when nondimensionalizing the isotropic Kuramoto–Sivashinsky continuity equation. We close this particular discussion by noting that the factor appearing before our sputtering yield constitutive relation and the dimension of the specific value of  $J_0$  should more properly have been  $h_0\ell_0^2$  per ion and ion cm<sup>-2</sup>sec<sup>-1</sup>, respectively, but since those quantities only appear in our formulation as their product  $w_n = J_0h_0\ell_0^2$ , in which case the ion designation cancels out, we did not explicitly indicate it for ease of exposition.

We complete the comparison of our model to previous ones by describing in more detail the damped Kuramoto-Sivashinsky evolution equation devised in [Facsko et al. 2004] mentioned earlier in relation to  $\lambda_0$ , the simulation of which could be used to model their original normal-incidence argon ion-sputtering gallium antimonide semiconductor quantum dot experiments. It differed from that of [Kahng et al. 2001] only owing to the presence of a nonzero white noise term  $\eta_0$  and a linear damping term equivalent in our dimensionless notation to  $2\beta h$ , which had been introduced ad hoc for the purpose of suppressing spatiotemporal chaos and interpreted as the continuum effect of the mechanism of redeposition of the sputtered material on the substrate surface. Facsko et al. [2004] asserted that in the case of a corrugated morphology a considerable amount of the sputtered particles hits the surface and is redeposited resulting in a net exchange of material from higher- to lower-lying regions. This mechanism, which tends to decrease both  $h_0$ , the maximum deviation of the interface from its mean planar position, and  $w_n$ , the normal velocity of erosion, was first described in [Michely and Comsa 1991] but had been ignored heretofore in modeling endeavors. Observe that the  $h_0$ -dependence of our formula  $w_n = J_0 h_0 \ell_0^2$ for the normal velocity of erosion is consistent with this interpretation. Neither that equation of [Facsko et al. 2004] nor the one employed in [Kahng et al. 2001] were able to produce patterns when  $\lambda_0 = 0$  since the only nonlinear term for each was proportional to this parameter and such nonlinearities are required for pattern formation. Thus our model is unified in the sense that with  $\lambda_0 = 0$ , or equivalently  $\alpha = 0$ , and  $0 < \beta < 1$ , it also accounts for the formation of ripples at normal incidence which those of [Kahng et al. 2001; Facsko et al. 2004] could not do.

Our results differ from those obtained in [Pansuwan et al. 2005] from their analysis of a related model equation for solid surface erosion caused by normal-incidence ion sputtering that did not include the simplifying approximation for the magnitude of its gradient. That analysis basically employed the more complicated

hexagonal planform method of weakly nonlinear stability theory (reviewed in Chapter 17 of [Wollkind and Dichone 2017]) to study pattern formation in this phenomenon and only used the easier to implement rhombic planform one to mediate these results by determining the parameter range for stable square patterns instead of generating all its pattern formation predictions as we do from our rhombic planform analysis. The reason for this was that since the Cangelosi et al. [2015] paradigm for lower- and higher-threshold patterns based upon the mean position of the interface as we do here had yet to be developed, the predicted zero-threshold results of their rhombic planform analysis could not be used to compare with experimental and simulated patterns. Our goal being to employ the simplest reasonable model and method of analysis that produce results in agreement with experimental data, we chose to perform that threshold-dependent rhombic planform analysis on the evolution equation derived in Section 1 rather than on the corresponding more complex one of [Pansuwan et al. 2005]. Further since [Facsko et al. 2004] was published simultaneously with [Pansuwan et al. 2005], the latter authors used the existing stochastic model of [Cuerno et al. 1995] for solid surface erosion via normal-incidence ion sputtering to estimate the value of  $\lambda_0/2$ , which they took to be equal to 0.01 nm/sec as opposed to our taking this as the value of  $2\lambda_0$ . Note that for the value of this parameter employed in [Pansuwan et al. 2005] the experiments of [Facsko et al. 1999] yielded  $\alpha \cong 1.788$ , which being greater than  $\alpha_2$  would lie outside our predicted range of  $0 < \alpha < \alpha_2 = 1.376$  for pattern formation.

In conclusion, this normal-incidence ion-sputtered erosion pattern-formation problem of a semiconductor or metallic solid interfacial surface, involving a single spatiotemporal partial-differential evolution equation, is compatible with the ultimate goal of comprehensive applied mathematical modeling of developing the simplest reasonable formulation which preserves the essential features of a phenomenon and is still in agreement with relevant observational or experimental data [Wollkind and Dichone 2017]. The basic theme of such modeling is that when its theoretical predictions are compared with this data from the phenomenon under investigation these predictions and that phenomenological data are self-consistent, hence validating the model. Paradoxically, achieving this required us to add a secondary yield term and introduce a gradient simplification in our model to make it both unified and more tractable for analysis, respectively.

## Acknowledgement

We would like to thank the National Science Foundation (NSF) for its financial support of Sydney Schmidt and Stephanie Kolden under the Center for Undergraduate Research in Mathematics (CURM) grant DMS-1722563 to their advisor Professor Bonni J. Dichone.

#### References

- [Cangelosi et al. 2015] R. A. Cangelosi, D. J. Wollkind, B. J. Kealy-Dichone, and I. Chaiya, "Non-linear stability analyses of Turing patterns for a mussel-algae model", *J. Math. Biol.* **70**:6 (2015), 1249–1294. MR Zbl
- [Chason et al. 1994] E. Chason, T. M. Mayer, B. K. Kellerman, D. T. McIlroy, and A. J. Howard, "Roughening instability and evolution of Ge(001) surface during ion sputtering", *Phys. Rev. Lett.* **72**:19 (1994), 3040–3043.
- [Cross and Hohenberg 1993] M. C. Cross and P. C. Hohenberg, "Pattern formation outside of equilibrium", *Rev. Modern Phys.* **65**:3 (1993), 851–1112. Zbl
- [Cuerno et al. 1995] R. Cuerno, H. A. Makse, S. Tomassone, S. T. Harrington, and H. E. Stanley, "Stochastic model for surface erosion via ion sputtering: dynamical evolution from ripple morphology to rough morphology", *Phys. Rev. Lett.* **75**:24 (1995), 4464–4467.
- [Davis et al. 2018] M. G. Davis, D. J. Wollkind, R. A. Cangelosi, and B. J. Kealy-Dichone, "The behavior of a population interaction-diffusion equation in its subcritical regime", *Involve* **11**:2 (2018), 297–309. MR Zbl
- [Facsko et al. 1999] S. Facsko, T. Dekorsy, C. Koerdt, C. Trappe, H. Kurz, A. Vogt, and H. L. Hartnagel, "Formation of ordered nanoscale semiconductor dots by ion sputtering", *Science* **285**:5433 (1999), 1551–1553.
- [Facsko et al. 2004] S. Facsko, T. Bobek, A. Stahl, H. Kurz, and T. Dekorsy, "Dissipative continuum model for self-organized pattern formation during ion-beam erosion", *Phys. Rev. B.* **69**:15 (2004), art. id. 153412.
- [Graham et al. 1994] M. D. Graham, I. G. Kevrekidis, K. Asakura, J. Lauterbach, K. Krischer, H.-H. Rotermund, and G. Ertl, "Effects of boundaries on pattern formation: catalytic oxidation of CO on platinum", *Science* **264**:5155 (1994), 80–82.
- [Kahng et al. 2001] B. Kahng, H. Jeong, and A.-L. Barabási, "Quantum dot and hole formation in sputter erosion", *Appl. Phys. Lett.* **78**:6 (2001), 805–807.
- [Kuramoto 1978] Y. Kuramoto, "Diffusion-induced chaos in reaction systems", *Progr. Theor. Phys. Suppl.* **64** (1978), 346–367.
- [Kuske and Matkowsky 1994] R. Kuske and B. Matkowsky, "On roll, square, and hexagonal cellular flames", *Eur. J. Appl. Math.* **5**:1 (1994), 65–93. Zbl
- [Landau 1944] L. Landau, "On the problem of turbulence", *Doklady Akad. Nauk SSSR* 44 (1944), 339–342. In Russian; translated in *C. R. (Dokl.) Acad. Sci. URSS* 44 (1944), 311–314. MR
- [Makeev and Barabási 1997] M. A. Makeev and A.-L. Barabási, "Ion-induced effective surface diffusion in ion sputtering", *Appl. Phys. Lett.* **71**:19 (1997), 2800–2802.
- [Makeev and Barabási 1998] M. A. Makeev and A.-L. Barabási, "Secondary ion yield changes on rippled interfaces", *Appl. Phys. Lett.* **72**:8 (1998), 906–908.
- [Makeev et al. 2002] M. A. Makeev, R. Cuerno, and A.-L. Barabási, "Morphology of ion-sputtered surfaces", *Nucl. Instr. Methods Phys. Res. Sect. B* **197**:3-4 (2002), 185–227.
- [Michely and Comsa 1991] T. Michely and G. Comsa, "Generation and nucleation of adatoms during ion bombardment of Pt(111)", *Phys. Rev. B* **44**:15 (1991), 8411–8414.
- [Pansuwan et al. 2005] A. Pansuwan, C. Rattanakul, Y. Lenbury, D. J. Wollkind, L. Harrison, I. Rajapakse, and K. Cooper, "Nonlinear stability analyses of pattern formation on solid surfaces during ion-sputtered erosion", *Math. Comput. Modelling* **41**:8-9 (2005), 939–964. MR Zbl
- [Rusponi et al. 1997] S. Rusponi, C. Boragno, and U. Valbusa, "Ripple structure on Ag(110) surface induced by ion sputtering", *Phys. Rev. Lett.* **78**:14 (1997), 2795–2798.

[Rusponi et al. 1998] S. Rusponi, G. Costantini, C. Boragno, and U. Valbusa, "Scaling laws of the ripple morphology on Cu(110)", *Phys. Rev. Lett.* **81**:19 (1998), 4184–4187.

[Rusponi et al. 1999] S. Rusponi, G. Costantini, F. Buatier de Mongeot, C. Boragno, and U. Valbusa, "Patterning a surface on the nanometric scale by ion sputtering", *Appl. Phys. Lett.* **75**:21 (1999), 3318–3320.

[Schmidt and Kolden 2020] S. Schmidt and S. Kolden, "Analysis of an evolution equation for a rhombic planform", student report, Gonzaga Univ., 2020, available at tinyurl.com/388cs47b.

[Segel 1966] L. A. Segel, "Non-linear hydrodynamic stability theory and its applications to thermal convection and curved flows", pp. 165–197 in *Non-equilibrium thermodynamics, variational techniques and stability* (Chicago, 1965), edited by R. J. Donnelly et al., Univ. Chicago Press, 1966. MR

[Sekimura et al. 1999] T. Sekimura, M. Zhu, J. Cook, P. K. Maini, and J. D. Murray, "Pattern formation of scale cells in lepidoptera by differential origin-dependent cell adhesion", *Bull. Math. Biol.* **61**:5 (1999), 807–828. Zbl

[Siegmann and Rubenfeld 1975] W. L. Siegmann and L. A. Rubenfeld, "A nonlinear model for double-diffusive convection", *SIAM J. Appl. Math.* **29**:3 (1975), 540–557. MR Zbl

[Sivashinsky 1977] G. I. Sivashinsky, "Nonlinear analysis of hydrodynamic instability in laminar flames, I: Derivation of basic equations", *Acta Astronaut.* **4**:11-12 (1977), 1177–1206. MR Zbl

[Swift and Hohenberg 1977] J. Swift and P. C. Hohenberg, "Hydrodynamic fluctuations at the convective instability", *Phys. Rev. A* **15**:1 (1977), 319–328.

[Walgraef 1997] D. Walgraef, Spatio-temporal pattern formation, Springer, 1997. Zbl

[Wollkind and Dichone 2017] D. J. Wollkind and B. J. Dichone, *Comprehensive applied mathematical modeling in the natural and engineering sciences*, Springer, 2017. MR Zbl

[Wollkind and Vislocky 1990] D. J. Wollkind and M. Vislocky, "An interfacial model equation for the bifurcation of solidification patterns during LPEE processes", *Earth-Sci. Rev.* **29**:1-4 (1990), 349–368.

[Wollkind et al. 1994] D. J. Wollkind, V. S. Manoranjan, and L. Zhang, "Weakly nonlinear stability analyses of prototype reaction-diffusion model equations", *SIAM Rev.* **36**:2 (1994), 176–214. MR Zbl

[Wollkind et al. 2008] D. J. Wollkind, F. J. Alvarado, and D. E. Edmeade, "Non-linear stability analyses of optical pattern formation in an atomic sodium vapour ring cavity", *IMA J. Appl. Math.* **73**:6 (2008), 902–935. MR Zbl

Received: 2020-06-28 Revised: 2020-09-30 Accepted: 2020-10-10

 $sydney\_schmidt\_ferris@hotmail.com$ 

Department of Mathematics, Gonzaga University,

Spokane, WA, United States

smkolden@hotmail.com Department of Mathematics, Gonzaga University,

Spokane, WA, United States

dichone@gonzaga.edu Department of Mathematics, Gonzaga University,

Spokane, WA, United States

dwollkind@wsu.edu Department of Mathematics, Washington State University,

Pullman, WA, United States





#### INVOLVE YOUR STUDENTS IN RESEARCH

*Involve* showcases and encourages high-quality mathematical research involving students from all academic levels. The editorial board consists of mathematical scientists committed to nurturing student participation in research. Bridging the gap between the extremes of purely undergraduate research journals and mainstream research journals, *Involve* provides a venue to mathematicians wishing to encourage the creative involvement of students.

#### MANAGING EDITOR

Kenneth S. Berenhaut Wake Forest University, USA

#### BOARD OF EDITORS

Colin Adams	Williams College, USA	Robert B. Lund	Clemson University, USA
Arthur T. Benjamin	Harvey Mudd College, USA	Gaven J. Martin	Massey University, New Zealand
•	,		• •
Martin Bohner	Missouri U of Science and Technology, USA	, ,	Colorado State University, USA
Amarjit S. Budhiraja	U of N Carolina, Chapel Hill, USA	Frank Morgan	Williams College, USA
Pietro Cerone	La Trobe University, Australia Mo	hammad Sal Moslehian	Ferdowsi University of Mashhad, Iran
Scott Chapman	Sam Houston State University, USA	Zuhair Nashed	University of Central Florida, USA
Joshua N. Cooper	University of South Carolina, USA	Ken Ono	Univ. of Virginia, Charlottesville
Jem N. Corcoran	University of Colorado, USA	Yuval Peres	Microsoft Research, USA
Toka Diagana	University of Alabama in Huntsville, USA	YF. S. Pétermann	Université de Genève, Switzerland
Michael Dorff	Brigham Young University, USA	Jonathon Peterson	Purdue University, USA
Sever S. Dragomir	Victoria University, Australia	Robert J. Plemmons	Wake Forest University, USA
Joel Foisy	SUNY Potsdam, USA	Carl B. Pomerance	Dartmouth College, USA
Errin W. Fulp	Wake Forest University, USA	Vadim Ponomarenko	San Diego State University, USA
Joseph Gallian	University of Minnesota Duluth, USA	Bjorn Poonen	UC Berkeley, USA
Stephan R. Garcia	Pomona College, USA	Józeph H. Przytycki	George Washington University, USA
Anant Godbole	East Tennessee State University, USA	Richard Rebarber	University of Nebraska, USA
Ron Gould	Emory University, USA	Robert W. Robinson	University of Georgia, USA
Sat Gupta	U of North Carolina, Greensboro, USA	Javier Rojo	Oregon State University, USA
Jim Haglund	University of Pennsylvania, USA	Filip Saidak	U of North Carolina, Greensboro, USA
Johnny Henderson	Baylor University, USA	Hari Mohan Srivastava	University of Victoria, Canada
Glenn H. Hurlbert	Virginia Commonwealth University, USA	Andrew J. Sterge	Honorary Editor
Charles R. Johnson	College of William and Mary, USA	Ann Trenk	Wellesley College, USA
K. B. Kulasekera	Clemson University, USA	Ravi Vakil	Stanford University, USA
Gerry Ladas	University of Rhode Island, USA	Antonia Vecchio	Consiglio Nazionale delle Ricerche, Italy
David Larson	Texas A&M University, USA	John C. Wierman	Johns Hopkins University, USA
Suzanne Lenhart	University of Tennessee, USA	Michael E. Zieve	University of Michigan, USA
Chi-Kwong Li	College of William and Mary, USA		· -

#### PRODUCTION Silvio Levy, Scientific Editor

Cover: Alex Scorpan

See inside back cover or msp.org/involve for submission instructions. The subscription price for 2021 is US \$205/year for the electronic version, and \$275/year (+\$35, if shipping outside the US) for print and electronic. Subscriptions, requests for back issues and changes of subscriber address should be sent to MSP.

Involve (ISSN 1944-4184 electronic, 1944-4176 printed) at Mathematical Sciences Publishers, 798 Evans Hall #3840, c/o University of California, Berkeley, CA 94720-3840, is published continuously online. Periodical rate postage paid at Berkeley, CA 94704, and additional mailing offices.

Involve peer review and production are managed by EditFLow® from Mathematical Sciences Publishers.

PUBLISHED BY

mathematical sciences publishers

nonprofit scientific publishing

http://msp.org/ © 2021 Mathematical Sciences Publishers



Square-free divisor complexes of certain numerical semigroup elements	1
JACKSON AUTRY, PAIGE GRAVES, JESSIE LOUCKS, CHRISTOPHER	
O'NEILL, VADIM PONOMARENKO AND SAMUEL YIH	
Minimizing closed geodesics on polygons and disks	11
IAN ADELSTEIN, ARTHUR AZVOLINSKY, JOSHUA HINMAN AND	
Alexander Schlesinger	
Factorizations of surjective maps of connected quandles	53
TORI BRAUN, CHARLOTTE CROTWELL, ALFRED B.H. LIU, PAUL	
Weston and David N. Yetter	
Strongly nonzero points and elliptic pseudoprimes	65
Liljana Babinkostova, Dylan Fillmore, Philip Lamkin,	
ALICE LIN AND CALVIN L. YOST-WOLFF	
The Chabauty space of $\mathbb{Q}_p^{\times}$	89
Antoine Bourquin and Alain Valette	
Generalized lattice-point visibility in $\mathbb{N}^k$	103
CAROLINA BENEDETTI, SANTIAGO ESTUPIÑAN AND PAMELA E.	
HARRIS	
Rhombic planform nonlinear stability analysis of an ion-sputtering evolution	119
equation	
SYDNEY SCHMIDT, STEPHANIE KOLDEN, BONNI DICHONE AND DAVID WOLLKIND	
On the Burau representation of $B_4$	143
Vasudha Bharathram and Joan Birman	
Solutions of the variational equation for an $n$ -th order boundary value	155
problem with an integral boundary condition	
BENJAMIN L. JEFFERS AND JEFFREY W. LYONS	
The cyclic graph (deleted enhanced power graph) of a direct product	167
DAVID G. COSTANZO, MARK L. LEWIS, STEFANO SCHMIDT, EYOB	
TSEGAVE AND GARE LIDELI	

